Triethylamine on Si(001)−(2 × 1) at 300 K: Molecular Adsorption and Site Configurations Leading to Dissociation

ARTICLE *in* THE JOURNAL OF PHYSICAL CHEMISTRY C · AUGUST 2012

Impact Factor: 4.77 · DOI: 10.1021/jp303002c

8 AUTHORS, INCLUDING:

J.-J. Gallet
Pierre and Marie Curie University - Paris 6
60 PUBLICATIONS **422** CITATIONS
SEE PROFILE

Rochet François
Pierre and Marie Curie University - Paris 6
111 PUBLICATIONS **1,973** CITATIONS
SEE PROFILE

Yves Borensztein
Pierre and Marie Curie University - Paris 6
106 PUBLICATIONS **1,510** CITATIONS
SEE PROFILE

Fausto Sirotti
CNRS & SOLEIL synchrotron
207 PUBLICATIONS **2,352** CITATIONS
SEE PROFILE

THE JOURNAL OF PHYSICAL CHEMISTRY C

Article

pubs.acs.org/JPCC

Triethylamine on Si(001)-(2 × 1) at 300 K: Molecular Adsorption and Site Configurations Leading to Dissociation

Ahmed Naitabdi,[†,‡,§] Fabrice Bournel,[†,⊥] Jean-Jacques Gallet,[†,⊥] Alexis Markovits,[∥] François Rochet,*[,†,⊥] Yves Borensztein,[‡] Mathieu G. Silly,[⊥] and Fausto Sirotti[⊥]

[†]Laboratoire de Chimie Physique Matière et Rayonnement, UMR 7614, CNRS, Université Pierre et Marie Curie, 11 rue Pierre et Marie Curie, 75005 Paris, France

[‡]Institut des NanoSciences de Paris, UMR 7588, CNRS, Université Pierre et Marie Curie, 4 place Jussieu, 75005 Paris, France

[§]Unité de Catalyse et de Chimie du Solide, UMR 8181, CNRS, Université de Lille 1, Bâtiment C3, 59655 Villeneuve d'Ascq, France

[∥]Laboratoire de Chimie Théorique, UMR 7616, CNRS, Université Pierre et Marie Curie, 4 place Jussieu, 75005 Paris, France

[⊥]Synchrotron SOLEIL, L'Orme des Merisiers, Saint-Aubin, BP 48, 91192 Gif sur Yvette Cedex, France

Supporting Information

ABSTRACT: We provide a comprehensive investigation of the adsorption of a tertiary amine molecule, triethylamine (TEA, $N(CH_2CH_3)_3$), on the Si(001)-(2 × 1) surface at room temperature (RT), using real-time synchrotron radiation X-ray photoemission (XPS) and scanning tunneling microscopy (STM), in combination with density functional theory (DFT) calculations. Real-time XPS measurements point to two consecutive reactions, the first one leading to the formation of a dative adduct, the second one to the conversion of the latter into a dissociated adduct via N−C bond cleavage (to give Si−$N(CH_2CH_3)_2$ and Si-CH_2CH_3 moieties). The kinetic model, that fits the experimental data, distinguishes unreactive dative bond molecules (forming a reservoir) from reactive ones, exchanged in a two-way reaction. At low coverage, the STM images show that the adsorption of a dative-bond TEA molecule induces a static buckling of the Si dimers, leading to the c(4 × 2) templating of the silicon surface. Approaching saturation coverage, dative bonded TEA molecules self-organize into c(4 × 2) domains, with an occupancy of one molecule per two dimers, and exhibit a ternary symmetry. While DFT points to two possible molecular conformations (staggered and eclipsed) with almost the same adsorption energy, only the eclipsed conformer is observed at RT. STM helps also in identifying sites and experimental conditions (pressure) that make the dissociation of TEA possible. At high dilution, dissociated molecules are systematically sitting as pairs on two adjacent dimers in a row. Remarkably, dissociated adducts do not induce static buckling, in stark contrast with the case of dative bonding. Close to surface saturation, the dative-to-dissociated conversion starts from the boundaries of dative-bond self-assembled c(4 × 2) domains, emphasizing the role of these domains as reservoirs of stable molecular adducts. Our data show also that the conversion reaction needs the presence of the gas phase and is accelerated by an increase of pressure.

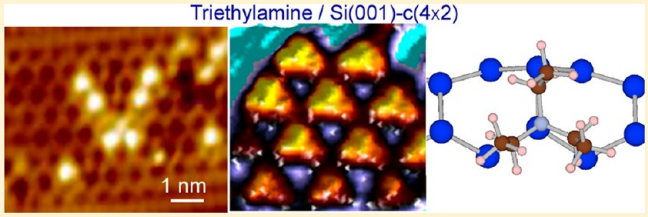

1. INTRODUCTION

Si(001) is one of the most studied semiconductor surfaces as a model system for the understanding of structural arrangement of the matter at the atomic scale. It is also extensively studied owing to its technological relevance in the current micro-electronic systems and in the promising and complex molecular electronics applications[1,2] when its surface is modified by molecular adsorbates. The reactivity of the Si(001) surface is dictated by its topology and the charge borne by the surface atoms.[3] Silicon atoms dimerize on the surface and form dimer rows along the [110] direction.[4−6] In addition, the dimers are buckled,[5,7−9] one atom moving upward, denoted Si-up (Si_u), while the other one moves downward, denoted Si-down (Si_d).[7] The electronic structure of this buckled surface is dominated by a negative charge transfer from the down Si_d dimer atom to the up Si_u dimer atom; thereby, the Si_d atom becomes electron-deficient (electrophilic), while the Si_u becomes electron-rich (nucleophilic). Below a transition temperature of ∼150 K, the static buckling leading to a c(4 × 2) reconstruction was observed in scanning tunneling microscopy (STM) images.[10,11] Bright protrusions arise from the Si_u (Si_d) dimer atom in the occupied (unoccupied) state STM images. Above the transition temperature, the dimer buckling becomes dynamic due to the fast thermally induced oscillations between up and down positions. In STM images, the dimers look symmetric and the surface appears (2 × 1) reconstructed, as oscillations occur at a time scale much smaller than the time resolution of STM experiments.

The zwitterionic nature of the silicon dimer suggests that surface reactions can be controlled by charges. In this respect,

Received: March 29, 2012
Revised: June 22, 2012
Published: June 25, 2012

the reaction of ammonia, and of primary, secondary, and tertiary amines with the Si(001) surface was the subject of numerous investigations, as, due to their nitrogen lone-pair, all these molecules are Lewis bases (electron-rich).[12−21] The nitrogen atom can indeed engage its lone-pair in the empty dangling bond of the Si_d dimer atom (an electron-poor, acidic site) to form a dative bonding (a Lewis acid−base reaction). In the case of ammonia, it has been shown that the dissociative adsorption takes place through a datively bonded intermediate state, followed by a N−H bond breaking and production of Si−NH_2 and Si−H moieties.[3,22]

The other amine molecules, such as methylamine (MA, $NH_2(CH_3)$),[14,15,17] dimethylamine (DMA, $NH(CH_3)_2$),[13,15−17] and trimethylamine (TMA, $N(CH_3)_3$),[13,15,16,19,23] proceed through a similar initial datively bonded adsorption state. The interaction of MA with the Si(001)-(2 × 1) surface has been shown to be dissociative via N−H bond cleavage, leading to the formation of Si−$NHCH_3$ and Si−H moieties.[14,15] According to density functional theory (DFT) cluster calculations, the N−H dissociation is kinetically more favorable than N−CH_3 bond cleavage.[14] Similarly, from DFT calculations[16,17] and experimental investigations, XPS,[13] Fourier transform infrared spectroscopy (FTIR),[13] auger electron spectroscopy (AES), and thermal desorption spectroscopy (TDS),[15] the DMA molecules undergo a dissociative adsorption on Si(001) at room temperature via N−H bond cleavage, facilitated by a low-energy activation barrier (E_b = 0.80 eV).[16] However, in contrast with primary and secondary amines, the molecular adsorption on Si(001) at room temperature via dative bonding was found stable for the tertiary amine, TMA, with minority species under the dissociative form.[13] At cryogenic temperatures (80 K), Hossain et al.[19,23] provided STM images of TMA molecularly chemisorbed on the buckled Si(001)-c(4 × 2) surface, showing that the adsorption is site specific: TMA bonds to empty, acidic Si_d sites, substantiating the dative bond picture. Cho and Kleinman[16] calculated a high (∼2 eV) activation barrier for N−C bond breaking (measured from the datively bonded state) and conjectured that the XPS identification of dissociated states at room temperature[13] was due to the reaction of the molecule on special sites of an unspecified nature.

Our study of another tertiary amine molecule, triethylamine (TEA), is motivated by the interest of comparing its reactivity on the silicon surface with that of other tertiary amines, especially the paradigmatic TMA. The reaction of TEA with the silicon surface could present substantial differences with respect to TMA, both at thermodynamic and kinetic levels. First, because the ethyl substituent is being more electron donating than the methyl group, the charge transfer to nitrogen in TEA should be larger than in TMA. This is indeed revealed by the gas basicity, stronger in TEA (951 kJ/mol) than in TMA (918.1 kJ/mol),[24] and by the binding energy of the nitrogen lone-pair (the highest occupied molecular orbital (HOMO)), found lower in TEA than in TMA.[25] Second, the nucleophilicity of TEA, i.e., its reaction kinetics with silicon electron-poor down dimer atom, may also be affected by ethyl substituent steric effects. In fact, as ethyl is bulkier than methyl, the trigonal pyramidal arrangement of bonds around the nitrogen atom is less pronounced in TEA than in TMA (in the C_3 symmetry TEA conformer, the ∠CNC angle is 113.4°,[26] while it is 110.5° in TMA[27]). In summary, TEA is a stronger base than TMA but a poorer nucleophile.

This article presents an original experimental investigation of TEA adsorbed at room temperature on the Si(001)-(2 × 1) surface, combined with the calculation of adsorption geometries via periodic slab DFT. Indeed, to facilitate electron spectroscopy and STM data interpretation, calculations of a variety of surface adducts (molecular and dissociated) were performed, with special attention to the surface patterns and molecular areal density, in line with previous studies on TMA.[16]

Regarding the experimental approach, we combined real-time synchrotron radiation X-ray photoemission and scanning-while-dosing STM measurements, from the initial stage of the deposition up to surface saturation. We examined the conditions (molecular areal density and TEA dosing pressure) that enable the formation of self-assembled domains of nondissociated, datively bonded molecules. We address the intriguing issue of molecular dissociation via N−C bond cleavage, which should be kinetically prohibited according to calculations,[16] considering both kinetics deduced from real-time XPS, and the evolution of the molecular overlayer as seen from real-time, in situ STM.

2. CALCULATION DETAILS

We performed periodic calculations based on DFT in the generalized gradient approximation (using the PW91 exchange-correlation functional) as implemented in the VASP code.[28−31] Plane-wave basis sets (with a kinetic energy cutoff of 400 eV) describe the valence electrons: one, four, and five electrons for the surface atoms, H, C, and N, respectively, and four electrons for Si. The core electrons were replaced by projector augmented wave (PAW) pseudopotential.[32,33] The relaxation of the atomic positions in the supercell took place until the subsequent energy steps were smaller than 0.001 eV. The geometry optimizations and the densities of states were computed sampling the Brillouin zone in 7 × 7 × 1 Monkhorst-Pack set for the c(4 × 2), in 2 × 4 × 1 set for the p(4 × 2) cell, and in 2 × 2 × 1 set for the p(4 × 4). Monopole, dipole, and quadrupole corrections to the energy were included along the direction perpendicular to the slab.

In all cases, the building block of the clean surface are asymmetric dimers, with an out-of-phase buckling of two adjacent rows, leading to a c(4 × 2) reconstruction. We used a six-layer slab. With the calculations being periodic in three dimensions, we imposed between two successive slabs a distance large enough (>10 Å) to prevent any noticeable interaction.

The c(4 × 2) unit cell of the clean surface contains eight surface Si atoms (four dimers). The first four Si layers were relaxed while the two Si bottom layers and the hydrogen layer were kept at the bulk positions. A geometry optimization performed with a 15 × 15 × 15 Monkhorst-Pack set ensuring very good energy convergence yields a bulk Si−Si distance of 2.37 Å, which is very close to the experimental value of 2.35 Å.[34] The calculation (c(4 × 2) cell) leads to buckled dimers, with a surface dimer bond-length of 2.36 Å and a buckling angle of 18.6°. These values are in excellent agreement with experimental data provided by surface X-ray diffraction (bond length of 2.37 ± 0.06 Å and buckling angle of 20 ± 3°)[35] and DFT calculations.[36−38]

We have changed the surface density of adsorbed molecules, expressed in monolayers (ML). One ML corresponds to a surface density of 6.8×10^{14} species/cm^2, that is the surface density of one (001) silicon plane. We have first used 4 × 2 cells. A c(4 × 2) molecular unit cell allowed us to examine

Table 1. Geometrical Outputs after Energy Minimization[a]

bonding type	molecular unit cell	Si−N bond length (Å)	∠CNC (deg)	∠CNC (deg)	∠CNC (deg)	reacted dimer bond length (Å)	reacted dimer buckling (deg)	adjacent dimer bond length (Å)	adjacent dimer buckling (deg)
eclipsed dative	c(4 × 2)	2.30	113.4	113.6	114.9	2.44	5.5	2.32	16.5
staggered dative	c(4 × 2)	2.14	112.9	113.7	115.9	2.43	5.2	2.34	16.5
dissociated	p(4 × 4)	1.76				2.46	0.23		

[a]We recall that the clean surface dimer bond-length is 2.36 Å, and its buckling is 18.6° (c(4 × 2) cell).[35−38]

molecular coverages of 0.5 ML (four molecules per unit cell, that is one molecule per dimer) and of 0.25 ML (2 molecules per unit cell, that is one molecule per two dimers). We also used a p(4 × 1) molecular unit cell corresponding to a nitrogen coverage of 0.125 ML (one molecule per unit cell, that is one molecule per four dimers). A larger p(4 × 4) molecular unit cell (16 surface silicon atoms) was also adopted to examine the nitrogen coverage of 0.125 ML (two molecules per unit cell), but in the latter case, we have an occupied/occupied/bare/bare/occupied/occupied sequence for the dimers along a row, instead of an occupied/bare/occupied sequence for the p(4 × 1) molecular unit cell.

The adsorption energies (E_{ads}) are written as $E_{ads} = E_{system} - (E_{Si} + E_{TEA})$, where E_{system} is the total energy of the adsorbate plus substrate system, E_{Si} the total energy of the clean dimerized surface, and E_{TEA} the total energy of the isolated TEA molecule. A negative value of E_{ads} corresponds to an exothermic reaction. We recall that the DFT total energies are evaluated for a certain volume of the unit cell. Thus, they correspond to the Helmholtz energy at zero temperature and neglect zero point vibrations.

3. EXPERIMENTAL DETAILS

The experiments were conducted in two independent ultrahigh vacuum (UHV) chambers, one dedicated to STM measurements, and the other one to synchrotron XPS measurements.[39,40] The Si(001) samples used for both experiments were cut from the same wafer (n^+ type, phosphorus doped with $N_D \approx 10^{19}$ atoms/cm; resistivity ≈ 0.003 Ω × cm). An identical cleaning procedure of the Si(001) samples was used in both sets of experiments. The Si(001) sample was first rinsed in isopropanol and dried under N_2 gas flow. Then, it was degassed in UHV at 690−700 °C for 22 h, before being cleaned from its native oxide by one flash annealing at 1150 °C (direct-current heating).

The TEA solution was purchased from Aldrich (99.99%) and purified by several freeze−pump−thaw cycles before dosing. The TEA molecules were introduced in the STM chamber through a UHV compatible fine leak-valve under constant pressure (background dosing). A similar procedure was used for XPS measurements. For both STM and XPS experiments, the TEA dosing on the Si(001) surface was done at room temperature.

The UHV system for STM measurements comprises two chambers (Preparation and Analysis (STM, Variable Temperature STM XA from Omicron NanoTechnology, Germany)), both of which exhibited pressures better than 3×10^{-11} mbar. During the Si(001) flashing procedure, the pressure did not exceed 1.5×10^{-10} mbar in the preparation chamber. The clean Si(001) sample was then transferred to the analysis chamber for STM experiments at room temperature. The occupied-states (unoccupied-states) STM images were obtained by a constant current mode of 100 pA and a sample voltage of −2 V (+2 V) at room temperature. A chemically etched tungsten tip, cleaned by heating in UHV was used.

XPS experiments were performed at TEMPO beamline, SOLEIL synchrotron (Saint Aubin, France).[39,40] The photon source is a HU80 Apple II undulator set to deliver linearly polarized light. The end-station is fitted with a modified 200 mm hemispheric electron analyzer (SCIENTA 200).[41] The electron take-off direction (respectively, the beam direction) was 0° (respectively, 44°), with respect to the surface normal. The polarization of the radiation was within the (110) plane of the silicon crystal. The photoemission spectra measured after exposure to TEA, were taken at photon energies ($h\nu$) of 530 eV (N 1s) and 335 eV (C 1s). The overall energy resolution, photon bandwidth, and electron analyzer was ∼100 meV (respectively, ∼250 meV) at a pass energy of 50 eV (respectively, 200 eV).

In order to get the kinetic information, real-time photoemission spectra were measured, while the surface was exposed to the TEA gas. The XPS core-level spectra, N 1s and C 1s, were acquired simultaneously at $h\nu$ = 530 eV. The electron analyzer was operated with a fixed retardation voltage for each binding energy region. The pass energy was set to 200 eV, as the energy range of a measured spectrum is determined by the active detector area in the energy dispersive direction, corresponding to ∼6% of the pass energy used.

The pressure gauges in the STM and XPS were not calibrated against one another. Therefore, the respective working background pressures during the dosing with TEA are noted P^{TEA}_{STM} and P^{TEA}_{XPS} respectively. In addition, STM images were recorded while dosing; thus, the effective pressure was certainly inferior to the background pressure P^{TEA}_{STM} due to shadowing by the tip.

4. RESULTS AND DISCUSSION

4.1. Computed Adsorption Geometries. We calculated the minimum energies for different adsorption geometries and various molecular coverages expressed in ML (0.5 ML of TEA corresponds to one molecule per one silicon dimer). The most relevant geometrical outputs (bond lengths and angles) are collected in Table 1, and E_{ads} are given in Table 2.

In the dative case, we tested two conformers; the staggered and the eclipsed one (see Figure 1). The c(4 × 2) molecular array with 0.5 ML coverage (one TEA per dimer) is unstable, as one TEA out of two desorbs, leaving a c(4 × 2) molecular array with 0.25 ML coverage (one molecule per two dimers). Indeed, at a molecular coverage of 0.25 ML, E_{ads} is of the order of −1 eV, similar to previous findings for TMA.[13,16,42] For the staggered and the eclipsed conformers depicted in Figure 1, E_{ads} are equal within 0.1 eV. Looking carefully at the eclipsed conformation geometry, it is worthwhile noticing that the two hydrogen atoms bound to the α carbon atom oriented toward silicon are not equivalent. One of them points to the silicon unraveling a possible interaction. In the dative mode and at

dx.doi.org/10.1021/jp303002c | J. Phys. Chem. C 2012, 116, 16473−16486

Table 2. Adsorption Energies (E_{ads}) Obtained from the VASP Method for the Dative Adsorption Mode of TEA on Si(001) at Various Coverages[a]

molecular unit cell	number of molecules per cell	molecular coverage (ML)	adsorption mode	E_{ads} (eV)
c(4 × 2)	4	0.5	eclipsed	unstable
c(4 × 2)	4	0.5	staggered	unstable
c(4 × 2)	2	0.25	dative eclipsed	−1.1
c(4 × 2)	2	0.25	dative staggered	−1.2
p(4 × 2)	1	0.125	dative eclipsed	−1.7
p(4 × 2)	1	0.125	dative staggered	−1.7
p(4 × 4)	2	0.125	dative staggered	−2.0
p(4 × 4)	2	0.125	dissociated	−3.5

[a]The clean surface reconstruction is c(4 × 2), that is, two adjacent dimer rows are buckled out of phase. One ML corresponds to the surface density of a (001) silicon plane.

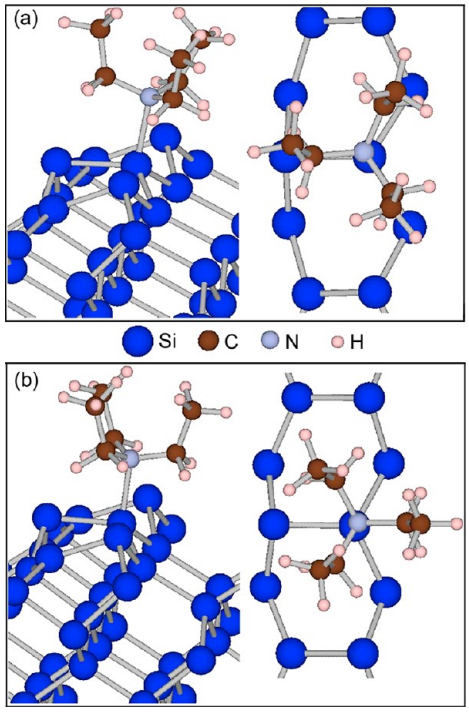

Figure 1. Excerpt from a c(4 × 2) molecular unit cell calculation (molecular coverage of 0.25 ML). The eclipsed (staggered) datively bonded conformer is shown in panel a (b). Perspective view (left-hand side) and top view (right-hand side, only the adsorbate and the first two silicon layers are shown). Note that only the eclipsed conformer is observed experimentally in locally self-assembled domains (coverage of 0.25 ML) in STM images (see section 4.3).

0.25 ML molecular coverage (see Table 1), the N−Si bond length is 2.30 Å (2.15 Å) for the eclipsed (staggered) conformer, and the ∠CNC angles are close to that of the free molecule (113.4°). The Si−Si dimer length is much longer (~2.44 Å) compared to that of the clean surface (2.36 Å). The TEA molecule is always bound to a Si down atom (Si_d), but the dimer buckling angle is 5.5° upon adsorption, much smaller than the 18.6° value obtained for the bare surface. The two adjacent dimers in the same row remain buckled (16.5°, slightly less than for the clean surface), as shown in Figure 1, with the Si up atoms (Si_u) as first neighbors of the adsorbed molecule.

Surface dilution increases E_{ads}, which reaches −1.7 eV (see Table 2) for a 0.125 ML coverage using a p(4 × 2) unit cell. This trend (E_{ads} = −2 eV) is confirmed by a calculation made for the same coverage of 0.125 ML, but with a different arrangement of the molecules. Using the large p(4 × 4) unit, we can place two datively bonded TEA molecules, diagonally opposed on two adjacent dimers of the same row (Figure 2).

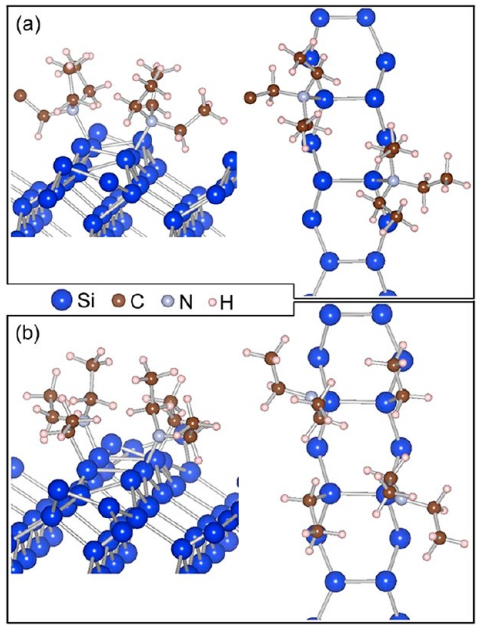

Figure 2. Excerpt from a p(4 × 4) unit cell calculation (molecular coverage of 0.125 ML). Adsorption sites involve two adjacent dimers of the same row. The dative mode (dissociated mode) is presented in panel a (b). Perspective view (left-hand side) and top view (right-hand side, only adsorbate and two first silicon layers are shown).

While at 0.5 ML (c(4 × 2) molecular unit cell), it was impossible to place two molecules on two adjacent dimers, it is clear that dilution allows it. Moreover, when comparing the two 0.125 ML calculations (p(4 × 2) and p(4 × 4)), E_{ads} is stronger when the two adsorbates sit on two adjacent dimers in the same row.

As expected, the dissociated mode yields the strongest interaction. We only examined the case of two dissociated molecules on two adjacent dimers, with the $SiN(C_2H_3)_2$ units located on alternating sides of the dimer row, as shown in Figure 2b. The dimer buckling (length) is 0.23° (2.46 Å), and the Si−N distance is 1.76 Å, much shorter than that for the dative bonded geometry (Table 2). We find E_{ads} = −3.5 eV for the p(4 × 4) cell at a coverage 0.125 ML, that is, 1.5 eV lower in energy than the corresponding nondissociated configuration. If the dissociation barrier could be overcome, then the equilibrium occupation of the dissociated state would be ~100% at 300 K. In fact the XPS and STM results (see below) show the coexistence of datively bonded molecules and dissociated ones, in line with the case of other amines on silicon surface.[13,17,43] As the complex issue of the energetic barriers encountered in the dissociation paths is beyond the scope of the present article, we cannot answer how C−N bond breaking occurs, but the experimental data presented in

dx.doi.org/10.1021/jp303002c | J. Phys. Chem. C 2012, 116, 16473−16486

sections 4.2 and 4.3 express the conditions for which the dissociation occurs.

4.2. Photoemission Results. Figure 3a shows the N 1s XPS spectrum of the Si(001)-(2 × 1) surface exposed to TEA,

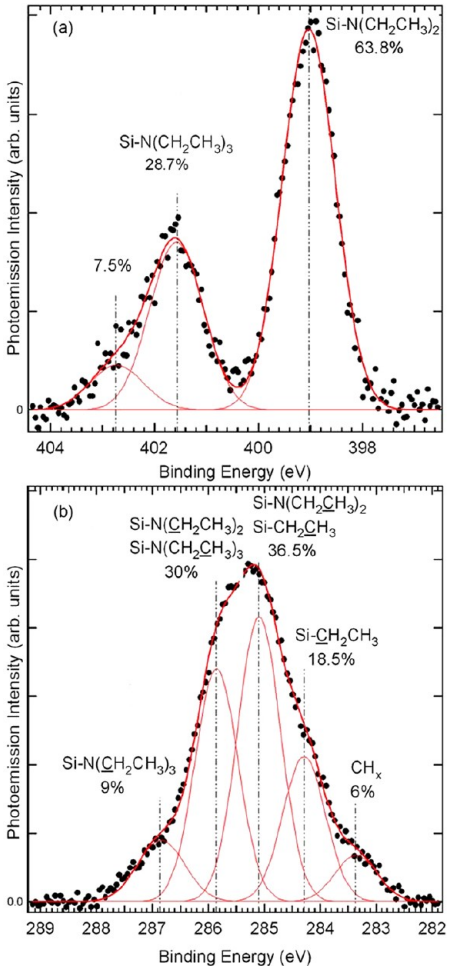

Figure 3. N 1s and C 1s core-level photoemission spectra of the Si(001)-(2 × 1) surface exposed to TEA at room temperature (the nominal pressure is P_{XPS}^{TEA} = 1.3 × 10^{-8} mbar and the exposure time 22 min, corresponding to 13 L). (a) Black circles: N 1s spectrum (hν = 530 eV, normal emergence) after background subtraction. Solid lines: fits with a sum of Gaussians. The component at 399 eV (64% of the spectral weight) is attributed to nitrogen atoms in dissociated adducts, that at 401.6 eV is attributed to nitrogen atoms in nondissociated, datively bonded, molecules (the small component at 402.7 eV accounts for the peak asymmetry of the datively bonded adduct). (b) Black circles: C 1s spectrum (hν = 335 eV, normal emergence) after background subtraction. Lines: result of the fit procedure with a sum of Gaussians (red solid lines). The fwhm is 0.9 eV for all components. The attribution of the various components is given in the figure (see also text).

at a nominal partial pressure of P_{XPS}^{TEA} = 1.3 × 10^{-8} mbar for 1320 s (corresponding to 13 L; 1 L = 10^{-6} Torr·s). The amount of nitrogen on the surface is deduced by comparison with the normalized N 1s XPS spectrum of the ammonia covered surface, following the procedure described in ref 21. A nitrogen surface density of 0.20 ML is measured (0.4 molecule per silicon dimer), close to the value of 0.24 ML measured by Cao and Hamers at room temperature (using also the ammonia-saturated surface standard as we do) for TMA,[13] and for the bulkier *N*,*N*-dimethylbutylamine.[43]

The N 1s spectrum exhibits two peaks that can be fitted by three Gaussians (full width at half-maximum, fwhm = 0.9 eV). The first is at ∼399 eV (64% of the spectra weight), the second at ∼401.6 eV (28.7%), and, in addition, a smaller component at 402.7 eV (7.5%), which accounts for the asymmetry of the peak at 401.6 eV.

The low binding energy (BE) peak at 399 eV is attributed to fragment species Si−N$(CH_2CH_3)_2$ resulting from the dissociation of TEA molecules via N−C bond cleavage. This BE assignment is consistent with the N 1s binding energies of ammonia (398.95 eV)[20] and primary/secondary amines (398.9 eV)[13,43] that are adsorbed dissociatively on the Si(001) surface. Thus, the dissociation of a TEA molecule has led to the formation of two fragments, Si−N$(CH_2CH_3)_2$ and Si-CH_2−CH_3, as deduced also from STM results (see Figure 7). The high BE peak at 401.6 eV is attributed to the datively bonded species Si−N$(CH_2CH_3)_3$. (For a discussion on the BEs of datively bonded amines on Si(001), see ref 21 where core-ionized state ΔKohn−Sham calculations are presented.) The BE of this component is close (smaller by 0.6 eV) to that found for the other tertiary amines TMA and *N*,*N*-dimethylbutylamine.[13,43] The small peak at 402.7 eV is also attributed to dative bond species but are found in an environment different from that of the molecules associated to the 401.6 eV component. The STM images (see section 4.3) show that dative bond molecules can form organized domains. A distribution of domain sizes might lead to variations in N 1s binding energies.

The corresponding C 1s spectrum is given in Figure 3b. It can be fitted with five components of fwhm equal to 0.9 eV, at 286.9 eV, 285.9 eV, 285.1 eV, 284.3 eV, and 283.4 eV. Hence, the overall energy resolution was sufficient to distinguish the carbon contribution in $-CH_2-$ (adjacent to the N atom) from the terminal $-CH_3$ carbon in the ethyl group (in the following, the core-ionized C is underscored). Our work on diaminobutane adsorbed dissociatively on Si(001)-(2 × 1), as the Si−NH−CH_2−CH_2−CH_2−CH_2−NH−Si component,[21] helps again to describe the C 1s spectrum of TEA molecules on Si(001). The C 1s spectrum of diaminobutane presents two peaks at 286.0 and 285.2 eV attributed (on the basis of core-ionized state ΔKohn−Sham calculations) to the two outer carbons (i.e., bonded to N) and to the two inner carbons of the aliphatic spacer, respectively. Therefore, the two main peaks at 285.9 and 285.1 eV are related to Si−N$(\underline{C}H_2CH_3)_2$ and Si−N$(CH_2\underline{C}H_3)_2$ of the dissociated molecule, respectively. The ethyl fragment bonded to Si is expected to appear at low binding energy (284.1 eV,[13] for Si-CH_3). Indeed, we found a component at 284.3 eV that we attributed to Si−$\underline{C}H_2CH_3$. The terminal CH_3 (Si−$CH_2\underline{C}H_3$) may also merge with the Si−N$(CH_2\underline{C}H_3)_2$ component at 285.1 eV, as the CH_2 moieties in cyclopentene adducts di-σ adsorbed on a silicon dimer are found at ∼284.8 eV.[44] The presence of the datively bonded species is represented by the component at 286.9 eV, which is attributed to Si−N$(\underline{C}H_2CH_3)_3$. As a matter of fact, datively bonded TMA is characterized by a sharp C 1s peak at the same BE.[13] The component related to Si−N$(CH_2\underline{C}H_3)_3$ should appear at lower BE than that of Si−N$(\underline{C}H_2CH_3)_3$. The calculated ionization potential of Si−$NH_2CH_2\underline{C}H_2CH_2CH_2NH_2$ (single-head datively bonded diaminobutane) was downshifted by 0.9 eV with respect to that of Si−$NH_2\underline{C}H_2CH_2CH_2CH_2NH_2$.[21] Therefore the Si−N-

dx.doi.org/10.1021/jp303002c | J. Phys. Chem. C 2012, 116, 16473−16486

$(CH_2CH_3)_3$ component could merge with that of Si–$N(CH_2CH_3)_2$. Finally, we noticed the presence of carbonaceous residues at 283.4 eV may be in relation with synchrotron beam damage.

The products of TEA reacting with Si(001) at room temperature resembles that of TMA and *N*,*N*-dimethylbutylamine at room temperature on the same surface, as judged from the sequential XPS measurements made by Cao and Hamers.[12,43] They also observe a mixture of datively bonded and dissociated species, the weight of the latter increasing at the expense of the former with increasing coverage. The relative weight of datively bonded molecules at saturation coverage is about 85% for TMA and 55% for *N*,*N*-dimethylbutylamine. Systematic kinetic studies should be conducted to examine whether C–N breaking is facilitated by the presence of long alkyl chains.

The adsorption kinetic of TEA was examined using real-time photoemission (Figure 4a,b), performed at room temperature under a TEA gas pressure of $P_{XPS}^{TEA} = 10^{-8}$ mbar for a total exposure of 1320 s, after which the leak valve was closed and the TEA gas was pumped down.

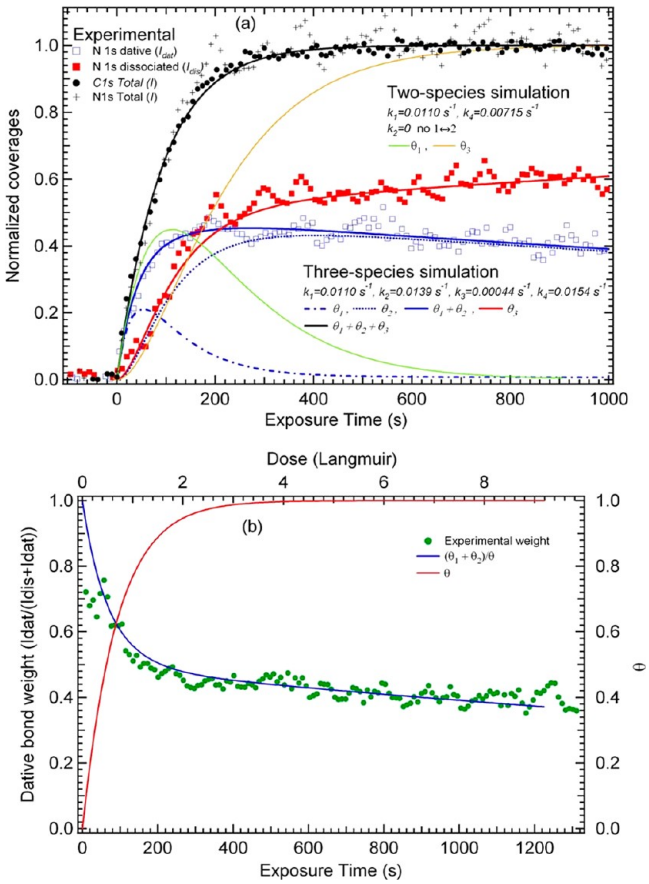

Figure 4. (a) Real-time photoemission measurement: N 1s (crosses) and C 1s (black filled circles) intensities as a function of time (normalized to 1 at saturation) for a Si(001) surface exposed to a TEA nominal pressure of 10^{-8} mbar at 300 K; dative bond (Si–$N(CH_2CH_3)_3$) component intensity (blue empty squares, I_{dat}) and dissociated geometry (Si–$N(CH_2CH_3)_2$) component (red filled squares, I_{dis}) as a function of time. The C 1s intensity curve is fitted with a Langmuirian curve $\theta(t) = 1 - \exp(-k_1 t)$ with $k_1 = 0.011$ s^{-1}. Simulation of adsorption kinetics with series of mechanisms leading to TEA dissociation are also plotted. (b) Spectral weight of the dative component (green filled circles) as a function of exposure (s) and dose (Langmuir). The simulation results $(\theta_2 + \theta_2)/\theta$ and θ ($\theta = \theta_1 + \theta_2 + \theta_3$) are also given for $k_1 = 0.011$ s^{-1}, $k_2 = 0.0139$ s^{-1}, $k_3 = 0.00044$ s^{-1}, and $k_4 = 0.0154$ s^{-1}.

The normalized C 1s and N 1s intensities are given in Figure 4a as a function of time t ($t = 0$ corresponds to the time at which the pressure of 10^{-8} mbar is reached). These intensities (I) are normalized to one at maximum coverage. The respective intensities of the N 1s dative bonding (I_{dat}) and dissociated (I_{dis}) species peak intensities are also given in Figure 4a. The N 1s dative bonding spectral weight is presented in Figure 4b, as a function of time and dose (expressed in Langmuir).

The C 1s and N 1s intensity curves show that, after an initial rapid uptake, surface saturation occurs after $t = 500$ s (corresponding to a dose of 4 L). The $I(t)$ curve can be fitted (Figure 4a) with a molecular fractional coverage function $\theta(t)$ of Langmuirian type (ignoring desorption)

$$\theta(t) = 1 - \exp(-k_1 t)$$

with $k_1 = 0.011$ s^{-1}; solution of the differential equation

$$\frac{d\theta}{dt} = k_1(1 - \theta) \quad (1)$$

,The reaction constant k_1 is equal to $S_0 \times F/N_{max}$, where S_0 is the initial sticking coefficient, N_{max} the molecular areal density at saturation, and F the molecular flux. The kinetic theory of gases states that $F = P/(2\pi m k_B T)^{1/2}$ where P is the pressure, m the mass of the molecule, k_B the Boltzmann constant, and T the temperature in Kelvin. As $F = 1.52 \times 10^{20} \times P_{XPS}^{TEA}$(mbar) molecules $\times$ cm$^{-2} \times$ s^{-1}, with $P_{XPS}^{TEA} = 10^{-8}$ mbar and $N_{max} = 0.2$ ML (1.36×10^{14} cm^{-2}), we find $S_0 = 0.98$, very close to unity.

The great advantage of in situ XPS is the monitoring of the dative and dissociated products as a function of time. Remarkably, the distribution of the surface species changes with time. Figure 4b show that the N 1s spectral weight of the dative bonding component $I_{dat}/(I_{dat} + I_{dis})$ is indeed equal to 0.70 ± 0.05 in the first 100 s of exposure (0.75 L; $I = 0.7$), then it decreases rapidly to 0.5 in the 100–200 s exposure range (0.75–1.5 L; $0.7 < I < 0.92$). Interestingly, the dative component weight continues to decrease slowly after surface saturation, below 0.5. This observation immediately eliminates a reaction scheme composed of two unimolecular parallel reactions (the I_{dat}/I_{dis} ratio should remain constant). In fact, the production of the dissociated species appears to be retarded: I_{dis} has a typical sigmoid-like shape, that is suggestive of two consecutive reactions assumed to be unimolecular

$$\text{TEA(gas)} \xrightarrow{k_1} \text{TEA(dative bond, coverage } \theta_1\text{) with } k_1 \text{ proportional to TEA pressure}$$

$$\text{TEA(dative bond, fractional coverage } \theta_1\text{)} \xrightarrow{k_4} \text{TEA(dissociated, fractional coverage } \theta_3\text{)}$$

The corresponding kinetic equations are

$$\frac{d\theta_1}{dt} = k_1(1 - \theta) - k_4\theta_1 \quad \text{with } \theta_1(t = 0) = 0 \quad (2)$$

$$\frac{d\theta_3}{dt} = k_4\theta_1 \quad \text{with } \theta_3(t = 0) = 0 \quad (3)$$

The closure equation is verified by

dx.doi.org/10.1021/jp303002c | J. Phys. Chem. C 2012, 116, 16473–16486

$$\frac{d(\theta_1 + \theta_3)}{dt} = \frac{d\theta}{dt} = k_1(1 - \theta)$$

which is identical to eq 1.

The solutions (for $k_1 \neq k_4$) of eqs 2 and 3 are two biexponentials (see the Supporting Information)

$$\theta_1(t) = \frac{k_1}{k_4 - k_1}(\exp(-k_1 t) - \exp(-k_4 t)) \quad \text{for } k_1 \neq k_4$$

$$\theta_3(t) = 1 - \exp(-k_1 t) - \theta_1$$

with $k_1 = 0.011\ s^{-1}$ (deduced experimentally from $I(t)$) and $k_4 \approx 0.00715\ s^{-1}$, the maximum of $\theta_1(t)$ (depending only on the ratio k_4/k_1) is 0.44, the maximum value reached by I_{dat}; see Figure 4a. This set of parameters provides the two simulated functions θ_1 and θ_3 plotted in Figure 4a, as a green and an orange thin solid curve, respectively. While the initial part of the I_{dat} and I_{dis} curves is relatively well reproduced by θ_1 and θ_3, the theoretical conversion of the dative bond species into the dissociated one occurs on a time scale much shorter than the one observed experimentally. Therefore, the problem must be reformulated, conserving the consecutive reaction scheme but taking into account that the dative species accumulates and slowly converts to the dissociated species. Indeed, Cho and Kleinman[16] have suggested that the conversion of the dative species to the dissociated one occurs on special sites, as the calculated dissociated barriers on normal sites are prohibitive. Formally, we can distinguish sites 1 where the conversion of the dative species (fractional coverage θ_1) to the dissociated one is possible, from sites 2 (fractional coverage θ_2) where the dative species is stored, with a reversible reaction between dative 1 and dative 2.

Assuming the following unimolecular reactions:

$$\text{TEA(gas)} \xrightarrow{k_1} \text{TEA(dative bond, dative 1, fractional coverage } \theta_1\text{)}$$

with k_1 proportional to TEA pressure

$$\text{TEA(dative 1, fractional coverage } \theta_1\text{)} \underset{k_3}{\overset{k_2}{\rightleftarrows}} \text{TEA(dative 2, fractional coverage } \theta_2\text{)}$$

$$\text{TEA(dative 1, fractional coverage } \theta_1\text{)} \xrightarrow{k_4} \text{TEA(dissociated, fractional coverage } \theta_3\text{)}$$

One obtains the corresponding kinetic equations

$$\frac{d\theta_1}{dt} = k_1(1 - \theta) - k_2\theta_1 + k_3\theta_2 - k_4\theta_1 \quad \text{with } \theta_1(t = 0) = 0 \tag{2'}$$

$$\frac{d\theta_2}{dt} = k_2\theta_1 - k_3\theta_2 \quad \text{with } \theta_2(t = 0) = 0 \tag{3'}$$

$$\frac{d\theta_3}{dt} = k_4\theta_1 \quad \text{with } \theta_4(t = 0) = 0 \tag{4'}$$

$$\frac{d(\theta_1 + \theta_2)}{dt} = k_1(1 - \theta) - k_4\theta_1 \tag{5'}$$

The closure equation is verified by

$$\frac{d(\theta_1 + \theta_2 + \theta_3)}{dt} = \frac{d\theta}{dt} = k_1(1 - \theta)$$

which is identical to eq 1; therefore, $\theta(t) = 1 - \exp(-k_1 t)$.

The equation set 1, 2′, 3′, 4′, and 5′ leads to triexponential solutions (see Supporting Information for the analytical calculation via Laplace transform):

$$\theta_1(t) + \theta_2(t) = A_{k_1}\exp(-k_1 t) + A_\alpha \exp(-\alpha t) + A_\beta \exp(-\beta t)$$

$$\theta_1(t) = B_{k_1}\exp(-k_1 t) + B_\alpha \exp(-\alpha t) + B_\beta \exp(-\beta t)$$

$$\theta_2(t) = C_{k_1}\exp(-k_1 t) + C_\alpha \exp(-\alpha t) + C_\beta \exp(-\beta t)$$

$$\theta_3(t) = 1 + D_{k_1}\exp(-k_1 t) + D_\alpha \exp(-\alpha t) + D_\beta \exp(-\beta t)$$

with

$$\alpha = \frac{1}{2}\left\{k_2 + k_3 + k_4 + \sqrt{(k_2 + k_3 + k_4)^2 - 4k_3k_4}\right\}$$

$$\beta = \frac{1}{2}\left\{k_2 + k_3 + k_4 - \sqrt{(k_2 + k_3 + k_4)^2 - 4k_3k_4}\right\}$$

$$\alpha > \beta > 0$$

and

$$A_{k_1} = \frac{-k_1(k_1 - k_2 - k_3)}{(k_1 - \alpha)(k_1 - \beta)},\ A_\alpha = \frac{k_1(\alpha - k_2 - k_3)}{(\alpha - \beta)(k_1 - \alpha)},\ A_\beta = \frac{-k_1(\beta - k_2 - k_3)}{(\alpha - \beta)(k_1 - \beta)}$$

$$B_{k_1} = \frac{-k_1(k_1 - k_3)}{(k_1 - \alpha)(k_1 - \beta)},\ B_\alpha = \frac{k_1(\alpha - k_3)}{(\alpha - \beta)(k_1 - \alpha)},\ B_\beta = \frac{-k_1(\beta - k_3)}{(\alpha - \beta)(k_1 - \beta)}$$

$$C_{k_1} = A_{k_1} - B_{k_1},\ C_\alpha = A_\alpha - B_\alpha,\ C_\beta = A_\beta - B_\beta$$

$$D_{k_1} = -1 - A_{k_1},\ C_\alpha = -A_\alpha,\ C_\beta = -A_\beta$$

These formulas are valid only when k_1 is different from α or β (for k_1 equal to α or β, see Supporting Information).

Considering that the dissociable (species 1) and stable (species 2) dative bond species are likely to have the same N 1s binding energy shift, then $I_{dat}(t)$ will be simulated by $\theta_1(t) + \theta_2(t)$ (the relative distribution of 1 and 2 is not accessible to the experiment). For its part, $I_{dis}(t)$ will be simulated by $\theta_3(t)$.

dx.doi.org/10.1021/jp303002c | J. Phys. Chem. C 2012, 116, 16473−16486

We first simulated $I_{dat}(t)$ by calculating $\theta_1 + \theta_2$. As A_{k1}, A_α, and A_β are functions of $k_{i\ (i=1,...,4)}$ and as k_1 is precisely measured from the fitting of $I(t)$ ($k_1 = 0.011\ s^{-1}$), only three parameters k_2, k_3, and k_4 must be varied to fit the $I_{dat}(t)$ curve. We obtain the best agreement for $k_2 = 0.0139\ s^{-1}$, $k_3 = 0.00044\ s^{-1}$, and $k_4 = 0.0154\ s^{-1}$, as shown in Figure 4a. Then, we calculated $\theta_3(t)$ with the same set of k_i (for self-consistency) and compared it with I_{dis}. The agreement is very good, as expected, because of the closure relationships $I_{dis}(t) = I(t) - I_{dat}(t)$ and $\theta_3(t) = \theta(t) - (\theta_1(t) + \theta_2(t))$. The calculated values of the pre-exponential factors are reported in Table 3. Besides k_1 ($k_1^{-1} = 91$ s), the characteristic inverse time constants (note they are independent of k_1) are α, the fast component equal to $0.0308\ s^{-1}$ ($\alpha^{-1} = 32$ s), and β, the slow component, equals $0.00023\ s^{-1}$ ($\beta^{-1} = 4350$ s). The present simulation leads to k_3 much smaller than k_2 and k_4. This means that the limiting step is the destorage of the stable species 2. The time dependence of θ_1 (the dissociable dative species 1) is practically a biexponential, as $B_\beta \approx 0$ and its maximum (at $t = 55$ s and $\theta = 0.46$) determines the inflection point of the sigmoid-like $\theta_3(t)$ function, that is its retard. For times greater than 300 s ($\theta > 0.96$), θ_1 is small compared to θ_2 and θ_3. Then, the dative contribution $\theta_1 + \theta_2$ is $\sim A_\beta \exp(-\beta t)$, with an inverse time constant $\beta \approx k_3(k_4/(k_3 + k_3))$.

Table 3. Characteristic inverse time constants and pre-exponential factors of θ_1+θ_2, θ_1 and θ_2 ($k_2 = 0.0139\ s^{-1}$, $k_3 = 0.00044\ s^{-1}$, $k_4 = 0.0154\ s^{-1}$). See text and figure 4a

inverse time constants (s^{-1})	time constants (s)	$\theta_1 + \theta_2$	θ_1	θ_2
$k_1 = 0.011$	$k_1^{-1} = 91$	$A_{k1} = -0.1840$	$B_{k1} = +0.5839$	$C_{k1} = -0.7679$
$\alpha = 0.0308$	$\alpha^{-1} = 32$	$A_\alpha = -0.3084$	$B_\alpha = -0.5894$	$C_\alpha = +0.2810$
$\beta = 0.00023$	$\beta^{-1} = 4350$	$A_\beta = +0.4924$	$B_\beta = +0.0086$	$C_\beta = +0.4838$

The kinetic approach, as all mean field theory approaches, does not give a microscopic description of the storage/destorage of the stable dative species 2 (that may include diffusion processes) nor does it explain how the molecule can dissociate in configurations of type 1. However, the scanning tunneling microscopy observations presented in the next subsection will provide elements that can be put in relation with the present phenomenological approach.

4.3. STM Results. *4.3.1. Molecular Adsorption at Low Coverage.* The clean Si(001) surface was first imaged prior to the TEA deposition (Figure 5a). As expected at room temperature, the surface exhibits apparently symmetric dimer rows along the [110]. Occasionally, static buckling is seen in the vicinity of defects.

A scanning-while-dosing procedure was used to follow the real-time adsorption of TEA molecules on the Si(001)-(2 × 1)

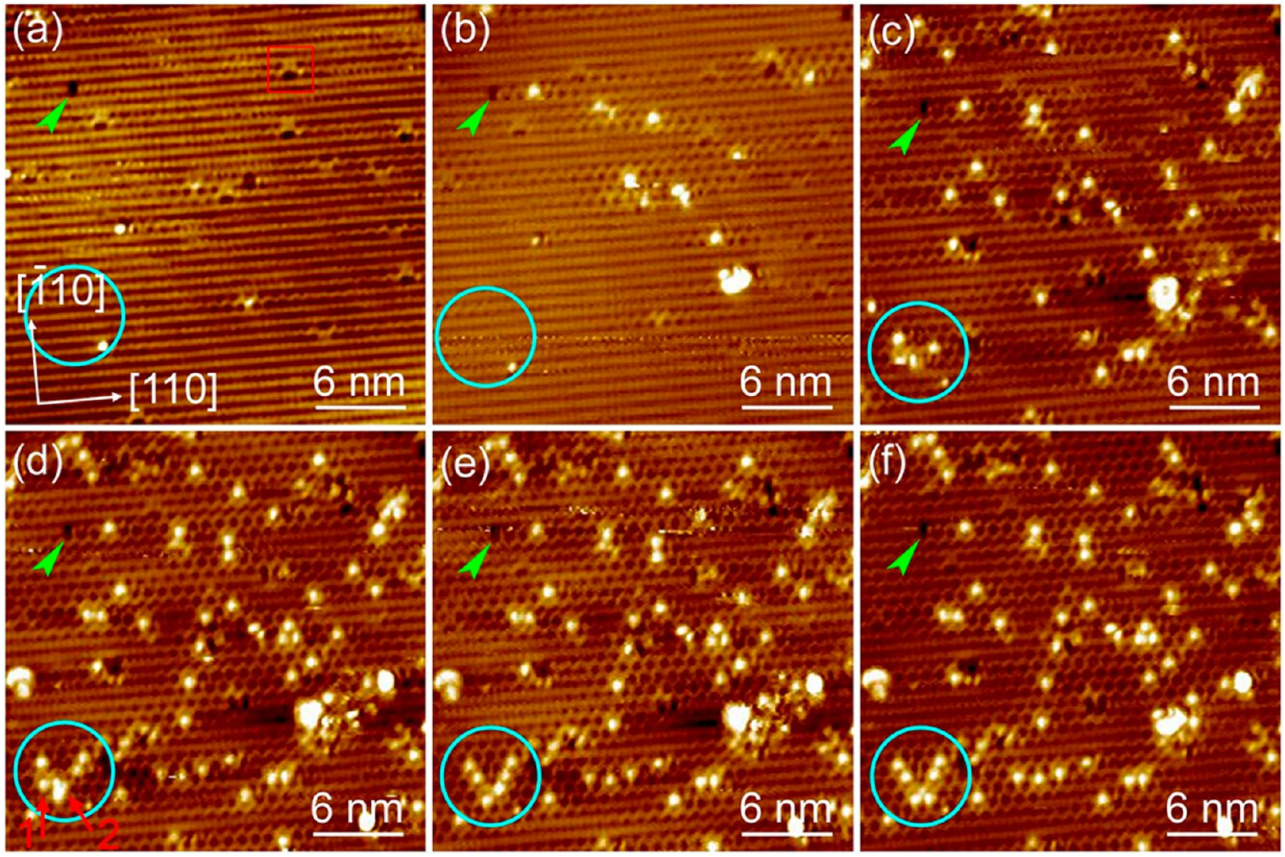

Figure 5. Consecutive STM images recorded on the same scan area of Si(001)-(2 × 1) surface at room temperature while dosing TEA: (a) clean surface before TEA dosing. Panels b, c, and d are snapshot images recorded while dosing (nominal dosing partial pressure of $P_{STM}^{TEA} = 5 \times 10^{-10}$ mbar) for 8 min. Panels e and f are recorded after the dosing was stopped. Total nominal exposure to TEA dosing: 0.18 L. The arrow points to a missing Si dimer used as a landmark. The open square indicates a *C*-defect (residual water dissociation). The open circle is used to monitor the evolution of the adsorption of the TEA molecules on the same area. Note the arising of the c(4 × 2) clean dimer domains with increasing TEA coverage. Tunneling conditions: $V = -2$ V; $I = 100$ pA.

dx.doi.org/10.1021/jp303002c | J. Phys. Chem. C 2012, 116, 16473−16486

surface. The scanning was kept on the same surface area throughout this first investigation, from the clean surface (before dosing) (Figure 5a) up to a surface exposed to a total nominal dosing of 0.18 L (8 min) (Figure 5f), the nominal dosing pressure P_{STM}^{TEA} being 5×10^{-10} mbar. Via this series of images, the adsorption sites, the nature of the molecular bonding, the mobility and stability of molecules, and the role of defects could be inferred.

Figure 5b shows individual bright protrusions on the Si dimer rows. We associate these molecular footprints to individual datively bonded molecules (i) because real-time XPS shows that this type of bonding is dominant at low coverage and (ii) because of the long-range static buckling associated with their appearance. This static buckling extends along the dimer row (at least over 6 nm) and in the perpendicular direction (typically the two dimer rows adjacent to the reacted one are also affected). The static buckling of bare dimers, along the dimer row surrounding the adsorbed molecules, is characteristic of dative bonding. A nearest neighbor Ising treatment of phosphine (PH_3) datively adsorbed on Si(001)-(2 × 1) shows that antisymmetric dimer ordering appears,[45] while it is not the case for dissociative adsorption (leading to SiH and $SiPH_2$ moieties). However, what is more surprising is the observation of buckling perpendicularly to the dimer rows, a situation not envisaged in ref 45. Figure 5b−f shows that the static buckling expands with increasing exposure to TEA molecules, together with an increased density of white protrusions. The surface in Figure 5d exhibits almost completely a c(4 × 2) pattern for a TEA coverage occupying only ∼0.6% of the total area. Therefore, the adsorption of a few TEA molecules on a dynamically buckled area of the Si(001)-(2 × 1) surface generates a static c(4 × 2) structure at room temperature. Comparable templating effects have been recently observed after adsorption of a dual-head tertiary amine, *N,N,N′,N′*-tetramethylethylenediamine on Si(001) surface.[46]

We devoted attention to the role that surface defects might play in the adsorption process, and possibly in dissociation events.[16] The first and more abundant type of defect is the so-called *C*-defect, appearing as a couple of depression and light protrusion on the same dimer row (an example is enclosed in a square in Figure 5a).[47−52] *C*-defects are the result of the dissociative adsorption of water on two adjacent dimers of the same row. Hossain et al. have shown that *C*-defects are more reactive than the bare dimers in the case of the dissociative adsorption of NH_3 on the Si(001) surface.[18] Here, the presence of a surface hydroxyl (SiOH) could steer the adsorption of TEA in its vicinity via hydrogen bonding with the nitrogen lone-pair. Figure 5a−c shows that *C*-defects do not act as preferential nucleation sites for TEA adsorption. The second and scarcer type of defect is the so-called single missing dimer defect (*A*-type defect).[8,53] It appears as an intrarow rectangular depression (see the arrow in Figure 5a). We do not see any preferential adsorption around these sites. The same is true for steps.

The scanning-while-dosing procedure allows us to determine the adsorption rate by counting the adsorption events in a given surface area, for a given time span. From a (50 nm × 50 nm) STM image, from which the image in Figure 5e was extracted, we counted 145 molecules after an exposure of 480 s under a nominal TEA pressure of 5×10^{-10} mbar, corresponding to a surface coverage of 5.8×10^{12} molecules/cm^2. In the framework of the kinetic theory of gases (taking the nominal TEA pressure), and assuming a sticking coefficient equal to one (see section 4.2), we would expect a surface coverage of 36.2×10^{12} molecules/cm^2. The observed molecule coverage is smaller than the expected one by a factor of 0.16. The discrepancy may be due to the shadowing of the scanned area by the STM tip. In fact, assuming an isotropic angle distribution of velocities for TEA molecules, a typical tip radius R of 500 Å (300 Å), and a surface-tip distance d = 5 Å, only a fraction $f = (1-(R/R + d)^2)^{1/2} \approx 0.14$ (0.18) of all incoming molecules will reach the scanning area in a straight line rather than hit the tip. Therefore, the actual pressure under the tip could be about an order of magnitude smaller than the nominal pressure P_{STM}^{TEA} measured in the chamber. This latter point may be of importance when comparison is made with the real-time XPS data.

The circled area of Figure 5 also illustrates the diffusion of molecules on the surface, besides the observation of successive adsorption events. The two molecules indicated by two arrows (1 and 2) in Figure 5d moved from their initial locations, toward new adsorption sites (Figure 5e,f). The hopping of TEA molecules observed here is independent of the scan direction, and thus, it is not mechanically induced by the tip.

The STM image in Figure 6a is a magnification of the light blue circled area in Figure 5f. We see that the molecules are adsorbed in a region where almost all bare dimers are statically buckled (Figure 5d), forming a c(4 × 2) domain. Each TEA molecule sits between two adjacent silicon atoms (on the same side of the dimer row) in the up position (Si_u), in accord with total energy calculations (section 4.1) indicating that a datively bonded molecule is indeed located between two Si_u atoms. The diffusion paths are shown in Figure 6b (dashed arrows). Jumps are observed both along the dimer rows and perpendicular to it, within a characteristic time-span of a few minutes. Surface mobility is a further evidence for a molecular, dative bonding adsorption mode. Surface diffusion barriers are substantially lower than the calculated desorption energy barriers E_a of the datively bonded molecule (as dative bonding is barrierless, E_a is equal to $-E_{ads}$ and thus ranges from 1.1 to 2.0 eV, according to coverage, see the DFT calculations of section 4.1). In fact, the residence time is $10^{-13}\exp(E_a/kT)$ corresponding to 10^6 s for E_a = 1.1 eV and 5×10^{21} s for E_a = 2.0 eV.

4.3.2. Molecular Dissociation at Low Coverage. We investigated the stability of adsorbed TEA molecules on Si(001) at low coverage. Figure 7 shows STM images acquired about two hours after the dosing was stopped, of the occupied states (unoccupied states); Figure 7a (7b). In addition to the molecularly adsorbed individual TEA molecules [square in Figure 7 a,c], several new features appeared on the surface [open circles in Figure 7a,c]. These new species represent 12% of the total number of molecules on the surface. They have a shelled-peanut shape, consisting systematically of two lobes placed diagonally on two adjacent dimers in the same row. Two orientations with equal distributions can be noticed for these diagonal features, the first (second) one, labeled *L* (*R*), is tilted 30° clockwise (anticlockwise) with respect to the dimer row direction. *R* and *L* are chiral structures with (110) being the mirror plane (perpendicular to the dimer row direction [110]); see Figure 7e,f.

The intensity profiles of the different species obtained through the line scan (i) and (ii) (Figure 7a−c) are plotted in Figure 7b−d. Configuration of *R* and *L* features (i) exhibit a large intensity in the occupied states STM image (Figure 7b) with apparent heights ($h_{R,L}$ = 1.6 Å) almost 3-fold higher than those of datively bonded molecules (ii) (h_D = 0.6 Å). In the

dx.doi.org/10.1021/jp303002c | J. Phys. Chem. C 2012, 116, 16473−16486

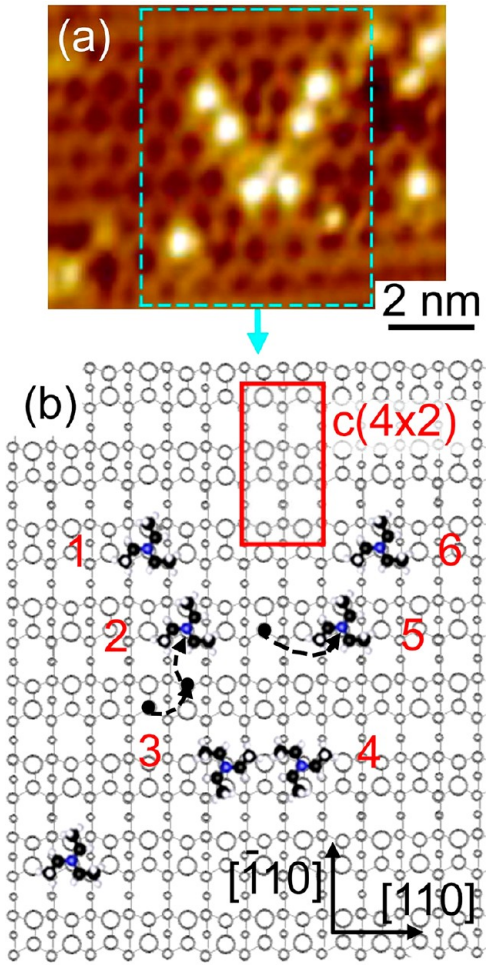

Figure 6. (a) Room temperature high-resolution STM image of TEA/Si(001) taken from the light blue circled area of Figure 5f. (b) Schematic model of the self-assembly of TEA molecules on Si(001), which shows also the formation of the c(4 × 2) reconstruction. This model corresponds to the area enclosed in the dashed rectangle drawn in panel a. The dashed arrows in panel b illustrate the displacement paths of the two molecules (1) and (2) from their initial positions as can be seen from Figure 5d to Figure 5e. Open circles are from large to small: Si up-dimer surface atom, Si down-dimer surface atom, Si 2nd layer atom, and Si 3rd layer atom. The shaded rectangle shows the surface unit cell c(4 × 2).

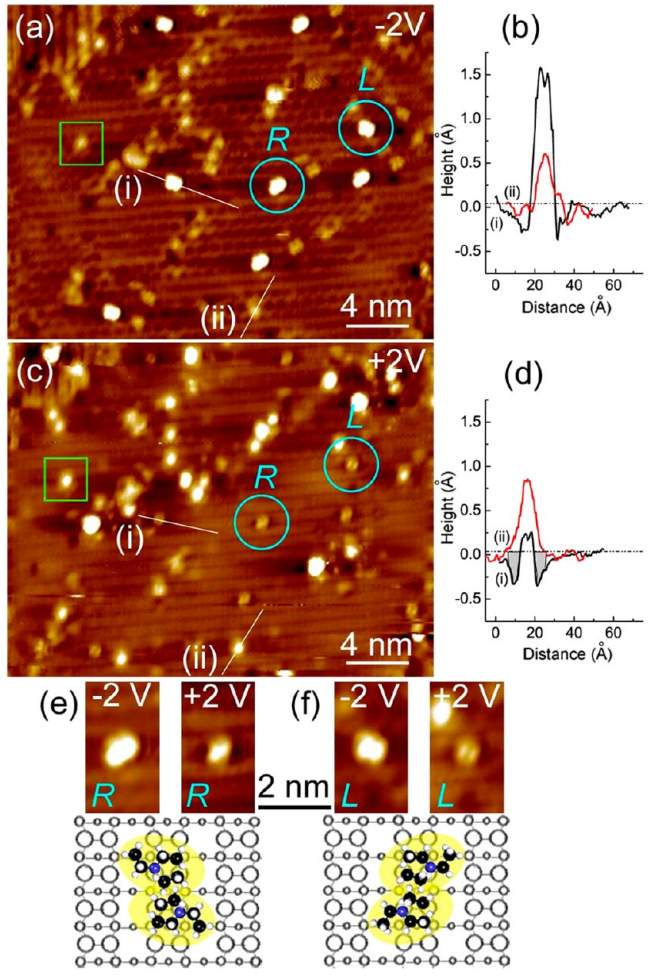

Figure 7. Panels a and c are occupied (V = −2 V, I = 100 pA) and unoccupied (V = +2 V, I = 100 pA) RT STM images of TEA on Si(001), respectively. They are consecutive images acquired on the same area. These images are recorded two hours after TEA dosing was stopped (0.18 L). Panels b and d are line-scans measured from occupied (a) and unoccupied (c) images, respectively as indicated: the black curve (i) is measured on the two dissociated TEA molecules; the red curve (ii) is measured on a single dative bond TEA molecule. The open square points to an example of single dative bond TEA molecule. Panel e (respectively, (f)) gives real STM images and corresponding schematic models of the remaining parts of two dissociated TEA molecules labeled R (respectively, L) as discussed in the text.

unoccupied states STM image, the apparent height for (L,R) species is $h_{R,L}$ = 0.2 Å nearly four times lower than that of a datively bonded TEA (h_D = 0.8 Å) (Figure 7d). There is thus a strong asymmetry of the electronic states of (R,L) fragments between the occupied and unoccupied state images. Consequently, the footprints of the (R,L) species are markedly different from those of the datively bonded species. Thus, we attribute R and L features to dissociated TEA molecules. Evidence for the presence of dissociated TEA has been shown in the XPS results (Figure 3) even at relatively low coverage (Figure 4). They are the result of N−C bond cleavage and formation of $Si{-}N(CH_2CH_3)_2$ and $Si{-}CH_2CH_3$ moieties. Another strong argument in favor of dissociation is the absence of static buckling in the dimer row on which (R,L) features are located. In the closely related case of phosphine adsorbed dissociatively on a silicon dimer, the Ising model calculation by Wilson and co-workers[45] show that, at room temperature, the free dimers are not statically buckled. The geometry of the dissociated adducts is depicted in Figure 2b. The terminal methyl carbons in the $Si{-}N(CH_2CH_3)_2$ and the $Si{-}CH_2CH_3$ moieties have a calculated height difference Δz of 1.75 Å that could manifest itself in the STM images. Tentatively, we attribute the brighter protrusions in occupied and unoccupied state images to the bulkier and higher $Si{-}N(CH_2CH_3)_2$ moiety.

As dissociated molecules are always paired, the present STM images suggest that the dative-to-dissociated state conversion may be not unimolecular, in other terms, dissociation of one molecule could be facilitated by the presence of a second molecule sitting on an adjacent dimer (maybe via a concerted path). In fact, during the two hours spent under UHV, there is ample time for a molecule wandering on the surface to find a partner. Equally, TEA molecules from the residual could be involved.

4.3.3. Self-Assembling Domains of Datively Bonded Molecules at High Coverage. Figure 8a displays a STM

dx.doi.org/10.1021/jp303002c | J. Phys. Chem. C 2012, 116, 16473−16486

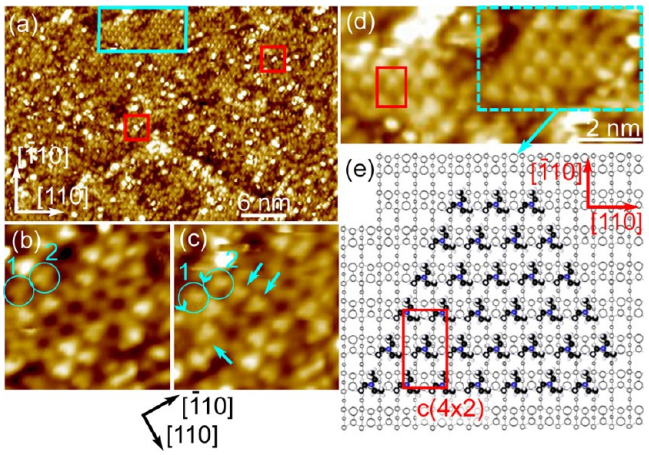

Figure 8. (a) Occupied states STM image ($V = -2$ V, $I = 100$ pA) of a high coverage TEA on Si(001)-(2 × 1) at RT recorded after increasing the TEA dosing pressure (P^{TEA}_{STM}) from 5×10^{-10} mbar (1.7 L) to 5×10^{-9} mbar (2.3 L). The two red open squares show an example of two dissociated TEA molecules *R* and *L*. Panels b and c are two consecutive high-resolution (5 nm ×5 nm) STM images acquired on the same area while dosing, to illustrate how the molecules adsorb on the induced c(4 × 2) surface area. The two images were acquired with a scanning angle of 45° with respect to the dimer row direction [110]. The open circles with arrows labeled 1 and 2 in panel c indicate two TEA molecules that have turned by ±180° rotation from their initial position in panel b followed by a translation of 3.84 Å (jump of the molecule to the next nearest dimer on the same row). The arrows in panel c indicate the positions of new molecules that arrived on the surface (relative to panel b). Panel d is a magnification image taken from the image (a) in the area indicated by an open rectangle and shows two well-ordered domains of TEA molecules. (e) Schematic model of the well-ordered domain of TEA corresponding to the area enclosed in the dashed rectangle drawn in panel d.

image of the Si(001) surface obtained after an exposure to 5×10^{-9} mbar pressure of TEA during 10.2 min (2.3 L, adding to the previous 1.7 L). The formation of locally well-ordered domains of molecularly adsorbed TEA molecules containing about 15 molecules is observed (rectangle in Figure 8a). Minority species, brighter than the datively bonded molecules, are also seen. Some (squares in Figure 8a) are the characteristic paired dissociated TEA molecules, *L* and *R*, already seen at low coverage (Figure 7). Some other bright footprints are unpaired, and may be attributed to isolated dissociated molecules.

Figure 8b,c is two consecutive high-resolution STM images acquired on a surface area where the remaining bare dimers are statically buckled c(4 × 2). While the molecular shape of an isolated adsorbed TEA molecule was unresolved at low coverage (Figure 6a), the adsorbed TEA molecules exhibit now, in the close-packed domain (Figure 8d), the clear ternary symmetry (three gray spots are observed), expected for the datively bonded adduct (see the calculated geometries in Figure 1, for which the $C_\alpha C_\beta$ bond axes point toward vacuum). We note that one triangle summit is systematically oriented toward the free atom of the reacted silicon dimer, corresponding to the eclipsed geometry of Figure 1a. At low coverage, the molecular footprints were more roundly shaped, due likely to the free rotation of the molecule around the Si−N axis. Indeed, total energy calculations indicated that the adsorption of eclipsed and staggered geometries (Figure 1a,b) is nearly degenerate (Table 2). Close packing apparently hinders that rotation, allowing the STM observation of the molecular symmetry.

The two successive images Figure 8b,c show how an ordered domain grows with the arrival of new molecules (arrows in Figure 8c). In particular, the pre-existing molecules labeled (1) and (2) cluster with the newcomers: they jump to the next dimer in the row and rotate by 180°, given that the TEA molecule must sit between two Si_u atoms. In Figure 8d, we present a well-ordered molecular domain that can be described by a c(4 × 2) cell (a schematic model of the molecular arrangement and the surface cell are shown in Figure 8e). The cell dimensions measured by STM are indeed ∼15.6 Å along [1̄10] and ∼7.9 Å along [110]. In the c(4 × 2) cell, one dimer in two is occupied, corresponding to a coverage of one molecule per two dimer (i.e., a molecular coverage of 0.25 ML). This corresponds exactly to the situation calculated in section 4.1 and depicted in Figure 1a.

4.3.4. Molecular Domain Stability: The Role of Pressure. The comparison between real-time XPS experiment (performed under a pressure P^{TEA}_{XPS} of 10^{-8} mbar) and the STM experiment (performed under nominal pressures P^{TEA}_{STM} in the 5×10^{-10}–5×10^{-9} mbar range) concurs in identifying two adsorption geometries, the dative bonding and the dissociated form. However, STM imaging tends to show that the dissociated form is a minority species at low coverage, while it represents about 60% of the species of the N 1s XPS spectra at surface saturation. Moreover, due to tip shadowing, effective pressures during STM measurements are smaller by a factor of 0.16 than the nominal ones. In fact, the pressure is a key parameter: kinetic simulations reported in the Supporting Information point to a strong dependence of the dative bond species weight at saturation coverage with the TEA pressure. Therefore, to examine a possible causal link between dissociation and pressure, we carried out the following sequences: (i) adsorption under a nominal pressure P^{TEA}_{STM} of 10^{-8} mbar, (ii) examination of the stability of the formed dative c(4 × 2) domains under ultra high vacuum (<10^{-10} mbar) for hours, and (iii) examination of the effect of a pressure surge of 5×10^{-8} mbar (the effective pressure of 0.8×10^{-8} mbar is now comparable to the TEA dosing pressure of the XPS measurements, which was $P^{TEA}_{XPS} = 1.8 \times 10^{-8}$ mbar) to look for possible changes in the dative/dissociated species distribution.

The STM image in Figure 9b was acquired using the scanning-while-dosing procedure (nominal P^{TEA}_{STM} of 1×10^{-8} mbar). A total effective dose of 7.6 L (17 min) led to the formation of molecular c(4 × 2) domains (open circle in Figure 9b) indicating that TEA molecules adsorb through dative bonding similarly to that observed at lower pressure P^{TEA}_{STM} (5×10^{-9} mbar). The organized domains contain tens of molecules, as in the preceding case. Their size can be limited by intrinsic aspects such as the molecular flux (the rate of arrival of molecules impinging on the surface and templating it) and/or by extrinsic ones, that is the density of defects on the starting surface. A detailed study of these aspects remains to be done.

The stability of the dative bond TEA molecules and the well-organized domains were monitored on this saturated surface after pumping the STM chamber down to a pressure below 1×10^{-10} mbar. Figure 9c,d displays STM images acquired 60 min and four hours after the dosing was stopped, respectively. We note that the dative bond domains appear stable under ultra high vacuum for observation times exceeding the characteristic dative bond component decay time β^{-1} (1.2 h) obtained from the real-time XPS study. Occasionally, their shape changes due to the mobility of the molecules on the surface, see the domains

dx.doi.org/10.1021/jp303002c | J. Phys. Chem. C 2012, 116, 16473−16486

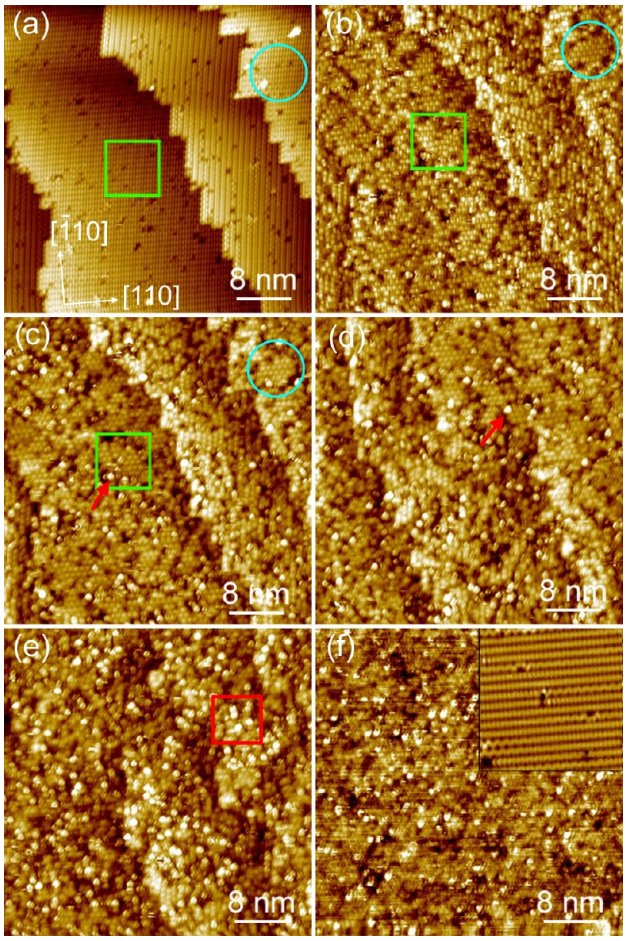

Figure 9. (a–f) Occupied states STM images ($V = -2$ V, $I = 100$ pA) at RT. (a) Clean Si(001)-(2 × 1) surface, (b) after 17 min of TEA at $P^{TEA}_{STM} = 1 \times 10^{-8}$ mbar acquired while dosing (total dose =7.6 L), and (c) 60 min after the dosing with TEA was stopped. The green square and the blue circle in panels b and c show well-organized TEA domains. The arrows indicate an isolated TEA molecules located in between well-ordered TEA domains, likely a dissociated species. (d) Four hours after the TEA dosing was stopped. (e) After additional exposure to TEA at $P^{TEA}_{STM} = 5 \times 10^{-8}$ mbar for 5 min. The square indicates dissociated TEA molecules. (f) Clean surface exposed to TEA under a pressure P^{TEA}_{STM} of 5×10^{-7} mbar for 5 min (clean surface in insert, 14.5 nm × 14.5 nm, showing the direction of the dimer rows).

within the blue and green marks. We note that the appearance of a few bright features, located at the boundaries of the ordered domains, in areas where the silicon surface is still bare, which we attribute to dissociated species (arrows in Figure 9c,d). They do not appear as pairs as in the low coverage case. The dissociated molecule weight estimated from Figure 9d is about 10%. The conversion of the dative to the dissociated geometry seems extremely slow when the TEA pressure is below 10^{-10} mbar. This suggests that the kinetic constant k_4 tends to zero when the TEA pressure goes to zero.

Figure 9e was obtained after an additional dosing of 5 min under a pressure P^{TEA}_{STM} of 5×10^{-8} mbar. A remarkable change in the adsorbed layer morphology is now observed. The average size of the c(4 × 2) molecular domain is reduced, while the areal density of dissociated TEA has strongly increased (the dissociated molecule weight is now 30%). This double trend change leads to an impression of increased disorder. Figure 9e confirms that dissociated molecules do not appear on adjacent dimer pairs. In Figure 9f, we show the image of a clean surface exposed to $P^{TEA}_{STM} = 5 \times 10^{-7}$ mbar for $\Delta t = 5$ min. The surface appears much more disordered than Figure 9b with no apparent c(4 × 2) TEA dative bond domains and thus is mainly covered by dissociated species. This series of experiments suggests that the conversion rate k_4 of the dative species increases with increasing pressure. Therefore, the assumption of a unimolecular conversion reaction, made in section B, may not be valid. As the reaction seems to be catalyzed by the presence of the gas phase, the reaction could be bimolecular, involving a physisorbed species TEA* in very low amounts (concentration proportional to P^{TEA}) on the surface compared to the chemisorbed species

$$\text{TEA(dative bond 1)} + \text{TEA*(gas phase or physisorbed)} \xrightarrow{k'_4} \text{TEA(dissociated)} + \text{TEA*(gas phase or physisorbed)}$$

Reactions on a surface assisted by the gas phase have been frequently studied as they play an important role in enhancing the chemical rates.[54] In the field of catalytic reactions, Shido et al. described a case of reaction intermediates being activated by the gas phase molecules. In particular, they examined the ethanol dehydrogenation on a dioxo-Nb monomer catalyst, for which the surface intermediate under the ambient gas was found to behave in a different way from that under vacuum.[54] The authors proposed that the Nb–ethanol intermediate complex (stable under vacuum) evolved to CH_3CHO and H_2 products only if a second molecule donated charge to the complex via its lone-pair. In the present study, the physisorbed TEA* could sit on a dimer adjacent to the one already occupied by a datively bonded TEA molecule, triggering the dissociation of these two molecules.

In this modeling, k_4 = constant should be replaced by $k_4 = k'_4 P^{TEA}$. The effect of k_1 and k_4 both proportional to P^{TEA} is examined in the Supporting Information (see Figure S2), where it is shown that the weight of the dative species decreases with increasing pressure at saturation.

To sum up, the STM experiments show that datively bonded molecules tend to cluster in ordered domains, with an occupancy of one molecule per two dimers. An occupancy of one molecule per dimer is not observed, in accord with DFT calculations. At very low coverage, the dissociated molecules always sit on two adjacent dimers. The possibility that adjacent dimer sites are occupied by dissociated molecules (also suggested by calculations) would lead to N_{max} = 0.5 ML (when all molecules are dissociated). In fact, XPS shows that N_{max} is around 0.2 ML at saturation, although the majority species (60%) are dissociated in agreement with the STM images showing that dissociation is no more correlated with adjacent dimer sites at high coverage. It suggests that, at high coverage, datively bonded molecules are converted into dissociated ones, leading to a saturation coverage close to that expected for dative adsorption. The microscopic view provided by STM can also help interpret the phenomenological approach described in section 4.2. The storage of inactive molecular species (constant k_2) could be interpreted as the formation of stable dative bond domains, the destorage (constant k_3) to active molecules being allowed by the mobility of the molecules. Active datively bonded molecules should be preferentially found at the periphery of the domains (where bare dimers are present), as dissociated species are found there.

dx.doi.org/10.1021/jp303002c | J. Phys. Chem. C 2012, 116, 16473–16486

5. CONCLUSIONS

By combining in situ synchrotron radiation XPS and STM with total energy calculations, based on a DFT periodic approach, we can draw a comprehensive picture of the reactivity of a tertiary amine like TEA on the Si(001)-2 × 1 surface at room temperature. The in situ experiments enabled us to examine both the nature of the chemical bonding and of the adsorption site, as a function of time and pressure. As other tertiary molecules, TEA is found both under a molecular form (datively bonded to Si) and a dissociated one. With respect to preceding works devoted to this family of molecules, the present study details the formation of self-assembled dative bond molecule arrays at room temperature and tackles the complex question of tertiary amine dissociation on Si(001). STM monitors the growth of dative bond clusters (via surface diffusion), leading to the formation of c(4 × 2)-ordered domains with an occupancy of one molecule per two dimers. In these domains, the 3-fold molecular symmetry is observed showing that the eclipsed geometry is preferred to the staggered one.

The conversion of molecular species into dissociated ones is observed by time-resolved N 1s photoemission, due to the large binding energy shift (2.6 eV) between the two chemical environments. A simple kinetic model based on unimolecular consecutive reactions accounts for the measured distribution of the respective products as a function of time. This model distinguishes two dative species, that can turn one into the other reversibly: one can dissociate, while the other is inactive. We show that the limiting step is the release of active dative species from the inactive dative species reservoir. In STM images, the height contrast between dative bond and dissociated species provides a clear distinction between these two adsorption geometries. STM shows that the dative bond domains are chemically stable in ultra high vacuum conditions (although their shape can change with time). However, the dative-to-dissociated conversion reaction is facilitated by increasing the pressure.

Our experimental work was supported by first-principles periodic DFT calculations of various adsorption geometries at various coverages using large cells (up to 4 × 4) that proved themselves useful in interpreting the XPS and STM data. In particular, calculations showed that adsorption energy (per molecule) of the dative bond species strongly depends on coverage. The calculation of dissociation paths was beyond the scope of the present work. Nevertheless, we believe that the experimental data collected here can help going a step further. The STM images tend to show that dissociation at the core of c(4 × 2) dative bond domains is difficult, in line with the work of Cho and Kleinman on TMA,[16] carried out for an occupancy of one molecule per two dimers. Therefore, the low coverage case, for which dissociated molecules pair up on adjacent dimers (may be via a concerted mechanism), should be addressed first, despite that very large cells are necessary. We also believe, that, in a second step, this relatively simple chemical system (with only two chemical products and no large modification of the silicon surface plane) is a very interesting object of study by dynamical approaches, whether for the growth and shape modification of the dative bond domains or for molecular dissociation occurring at the moving boundary of these domains in the presence of the gas phase.

■ ASSOCIATED CONTENT

Supporting Information

Resolution of the differential equations via Laplace transform method and simulation results for θ (the overall fractional coverage) and $\theta_1 + \theta_2$ (the overall dative contribution) as a function of kinetic parameters. This material is available free of charge via the Internet at http://pubs.acs.org.

■ AUTHOR INFORMATION

Corresponding Author

*E-mail: francois.rochet@upmc.fr.

Notes

The authors declare no competing financial interest.

■ ACKNOWLEDGMENTS

We thank Debora Pierucci for her helpful contribution during her summer internship in our group. We gratefully acknowledge useful discussions with Dr. Nathalie Capron of Université Pierre et Marie Curie, Paris 6, Paris, France.

■ REFERENCES

(1) Wolkow, R. A. *Annu. Rev. Phys. Chem.* **1999**, *50*, 413−441.
(2) Filler, M. A.; Bent, S. F. *Prog. Surf. Sci.* **2003**, *73*, 1−56.
(3) Yoshinobu, J. *Prog. Surf. Sci.* **2004**, *77*, 37−70.
(4) Murata, Y.; Kubota, M. *Phase Transitions* **1995**, *53*, 125−141.
(5) Ramstad, A.; Brocks, G.; Kelly, P. J. *Phys. Rev. B* **1995**, *51*, 14504−14523.
(6) Schlier, R. E.; Farnsworth, H. E. *J. Chem. Phys.* **1959**, *30*, 917−926.
(7) Chadi, D. J. *Phys. Rev. Lett.* **1979**, *43*, 43−47.
(8) Hamers, R. J.; Tromp, R. M.; Demuth, J. E. *Phys. Rev. B* **1986**, *34*, 5343−5357.
(9) Srivastava, G. P. *Comput. Phys. Commun.* **2001**, *137*, 143−162.
(10) Tochihara, H.; Amakusa, T.; Iwatsuki, M. *Phys. Rev. B* **1994**, *50*, 12262−12265.
(11) Wolkow, R. A. *Phys. Rev. Lett.* **1992**, *68*, 2636−2639.
(12) Widjaja, Y.; Mysinger, M. M.; Musgrave, C. B. *J. Phys. Chem. B* **2000**, *104*, 2527−2533.
(13) Cao, X. P.; Hamers, R. J. *J. Am. Chem. Soc.* **2001**, *123*, 10988−10996.
(14) Kato, T.; Kang, S. Y.; Xu, X.; Yamabe, T. *J. Phys. Chem. B* **2001**, *105*, 10340−10347.
(15) Carman, A. J.; Zhang, L. H.; Liswood, J. L.; Casey, S. M. *J. Phys. Chem. B* **2003**, *107*, 5491−5502.
(16) Cho, J. H.; Kleinman, L. *Phys. Rev. B* **2003**, *68*, 245314.
(17) Mui, C.; Wang, G. T.; Bent, S. F.; Musgrave, C. B. *J. Chem. Phys.* **2001**, *114*, 10170−10180.
(18) Hossain, M. Z.; Yamashita, Y.; Mukai, K.; Yoshinobu, J. *Phys. Rev. B* **2003**, *68*, 235322.
(19) Hossain, M. Z.; Machida, S.; Nagao, M.; Yamashita, Y.; Mukai, K.; Yoshinobu, J. *J. Phys. Chem. B* **2004**, *108*, 4737−4742.
(20) Mathieu, C.; et al. *Phys. Rev. B* **2009**, *79*, 205317.
(21) Mathieu, C.; et al. *J. Phys. Chem. C* **2009**, *113*, 11336−11345.
(22) Queeney, K. T.; Chabal, Y. J.; Raghavachari, K. *Phys. Rev. Lett.* **2001**, *86*, 1046−1049.
(23) Hossain, M. Z.; Machida, S.; Yamashita, Y.; Mukai, K.; Yoshinobu, J. *J. Am. Chem. Soc.* **2003**, *125*, 9252−9253.
(24) Hunter, E. P. L.; Lias, S. G. *J. Phys. Chem. Ref. Data* **1998**, *27*, 413−656.
(25) Bush, B.; Craig, J. H.; Roos, K. R.; Lozana, J.; Field, K. W. *Surf. Interface Anal.* **2008**, *40*, 927−930.
(26) Takeuchi, H.; Kojima, T.; Egawa, T.; Konaka, S. *J. Phys. Chem.* **1992**, *96*, 4389−4396.
(27) Murphy, W. F.; Zerbetto, F.; Duncan, J. L.; Mckean, D. C. *J. Phys. Chem.* **1993**, *97*, 581−595.
(28) Kresse, G.; Furthmuller, J. *Phys. Rev. B* **1996**, *54*, 11169−11186.

(29) Kresse, G.; Furthmuller, J. *Comput. Mater. Sci.* **1996**, *6*, 15−50.
(30) Kresse, G.; Hafner, J. *Phys. Rev. B* **1993**, *47*, 558−561.
(31) Kresse, G.; Hafner, J. *Phys. Rev. B* **1994**, *49*, 14251−14269.
(32) Blochl, P. E. *Phys. Rev. B* **1994**, *50*, 17953−17979.
(33) Kresse, G.; Joubert, D. *Phys. Rev. B* **1999**, *59*, 1758−1775.
(34) O'Mara, W. C.; Herring, R. B.; Hunt, L. P., Eds. *Handbook of Semiconductor Silicon Technology*; William Andrew Publishing: New York, 1990; pp 349−352.
(35) Takahasi, M.; Nakatani, S.; Ito, Y.; Takahashi, T.; Zhang, X. W.; Ando, M. *Surf. Sci.* **1995**, *338*, L846−L850.
(36) Zhou, J. G.; Hagelberg, F.; Xiao, C. Y. *Phys. Rev. B* **2006**, *73*, 155307.
(37) Demirel, G.; Cakmak, M.; Caykara, T.; Ellialtioglu, S. *J. Phys. Chem. C* **2007**, *111*, 15020−15025.
(38) Jung, S. C.; Kang, M. H. *Phys. Rev. B* **2009**, *80*, 235312.
(39) Beamline Description. http://www.synchrotron-soleil.fr/Recherche/LignesLumiere/TEMPO/DescriptionLigne.
(40) Polack, F.; et al. *AIP Conf. Proc.* **2010**, *1234*, 185−188.
(41) Bergeard, N.; et al. *J. Synchrotron Radiat.* **2011**, *18*, 245−250.
(42) Coustel, R.; Carniato, S.; Boureau, G. *J. Chem. Phys.* **2011**, *134*, 234708.
(43) Cao, X. P.; Hamers, R. J. *J. Vac. Sci. Technol., B* **2002**, *20*, 1614−1619.
(44) Khaliq, A.; Pierucci, D.; Tissot, H.; Gallet, J. J.; Bournel, F.; Rochet, F.; Silly, M.; Sirotti, F. *J. Phys. Chem. C* **2012**, *116*, 12680−12686.
(45) Wilson, H. F.; Marks, N. A.; McKenzie, D. R. *Surf. Sci.* **2005**, *587*, 185−192.
(46) Hossain, M. Z.; Mukai, K.; Yamashita, Y.; Kawai, H.; Yoshinobu, J. *Chem. Commun.* **2011**, *47*, 10392−10394.
(47) Cho, J. H.; Kim, K. S.; Lee, S. H.; Kang, M. H. *Phys. Rev. B* **2000**, *61*, 4503−4506.
(48) Hossain, M. Z.; Yamashita, Y.; Mukai, K.; Yoshinobu, J. *Phys. Rev. B* **2003**, *67*, 153307.
(49) Konecny, R.; Doren, D. J. *J. Chem. Phys.* **1997**, *106*, 2426−2435.
(50) Raghavachari, K.; Chabal, Y. J.; Struck, L. M. *Chem. Phys. Lett.* **1996**, *252*, 230−235.
(51) Okano, S.; Oshiyama, A. *Surf. Sci.* **2004**, *554*, 272−279.
(52) Yu, S. Y.; Kim, H.; Koo, J. Y. *Phys. Rev. Lett.* **2008**, *100*, 036107.
(53) Yokoyama, T.; Takayanagi, K. *Phys. Rev. B* **1997**, *56*, 10483−10487.
(54) Shido, T.; Yamaguchi, A.; Asakura, K.; Iwasawa, Y. *J. Mol. Catal. A: Chem.* **2000**, *163*, 67−77.